Development 128, 3975-3986 (2001)
Printed in Great Britain © The Company of Biologists Limited 2001
DEV2726

Severe nasal clefting and abnormal embryonic apoptosis in Alx3/Alx4 double mutant mice

Annemiek Beverdam, Antje Brouwer, Mark Reijnen, Jeroen Korving and Frits Meijlink*

Hubrecht Laboratory, Netherlands Institute for Developmental Biology, PO Box 85164, 3508AD Utrecht, The Netherlands
*Author for correspondence (e-mail: frits@niob.knaw.nl)

Accepted 18 July 2001

SUMMARY

A group of mouse aristaless-related genes has been implicated in functions in the development of the craniofacial skeleton. We have generated an *Alx3* mutant allele in which the *lacZ* coding sequence is inserted in-frame in the *Alx3* gene and the sequences encoding the conserved protein domains are deleted. Mice homozygous for this null allele are indistinguishable from wild-type mice. Compound mutants of *Alx3* and *Alx4*, however, show severe craniofacial abnormalities that are absent in *Alx4* single mutants. *Alx3*/*Alx4* double mutant newborn mice have cleft nasal regions. Most facial bones and many other neural crest derived skull elements are malformed, truncated or even absent. The craniofacial defects in *Alx3*/*Alx4* double mutant embryos become anatomically manifest around embryonic day 10.5, when the nasal processes appear to be abnormally positioned. This most probably leads to a failure of the medial nasal processes to fuse in the facial midline and subsequently to the split face phenotype. We detected a significant increase in apoptosis localised in the outgrowing frontonasal process in embryonic day 10.0 double mutant embryos, which we propose to be the underlying cause of the subsequent malformations.

Key words: Cleft face, Homeobox gene, Craniofacial development, Apoptosis, Mouse, Aristaless-related genes, Cephalic neural crest, Strong's luxoid, Limb development

INTRODUCTION

The vertebrate skull is classically subdivided in chondro-, neuro- and viscerocranium, which have different embryonic and evolutionary origins. Based on lineage studies in avian embryos, Couly et al. (Couly et al., 1993) recognise a 'chordal' and a 'prechordal' (or 'achordal') skull. While the chordal skull is derived from paraxial and cephalic mesoderm, the prechordal skeleton is entirely derived from the cephalic neural crest (reviewed by LeDouarin et al., 1993). This implies that the bones and connective tissues of the vertebrate face originate entirely from neural crest-derived tissues.

Facial development starts with the emergence of the five facial primordia: the frontonasal process and the paired mandibular and maxillary processes that are derived from the mandibular arch. These processes consist mainly of neural crest-derived mesenchyme covered by epithelium. Outgrowth of the primordia occurs through controlled proliferation of mesenchymal cells, which depends in part on signalling from the overlying epithelium (Wedden, 1987; Richman and Tickle, 1992). As the facial prominences grow out, the nasal processes fuse in the midline with each other and laterally with the maxillary processes. Frequently occurring facial cleft disorders, as known from human pathology and several mouse mutant models, are in many cases thought to result from these fusion events going awry (reviewed by Thorogood, 1997).

Morphogenesis of neural crest-derived structures depends on the integrated action of several types of patterning genes (reviewed by Schilling, 1997). Genes responsible for early anteroposterior patterning of the central nervous system, e.g. Hox and Otx genes, are to some extent responsible for the pre-programming of neural crest cells as they emigrate from the neural tube. Many other genes, including members of different homeobox gene families, exert their function in the mesenchymal cells that populate the facial processes. Other genes encode signalling factors, including members of the Fgf and Wnt families and sonic hedgehog (*Shh*) are locally expressed in the epithelia that cover the processes or in adjacent endoderm. Crosstalk between these two types of gene is likely to underlie in many cases the reciprocal epitheliomesenchymal interactions known to be crucial in the development of the craniofacial skeleton (Ferguson et al., 2000). Aristaless-like homeobox genes form a distinct gene family whose members are characterised by a paired type homeobox and the presence of a small conserved C-terminal domain in the proteins encoded, known as aristaless or OAR domain; see review by Meijlink (Meijlink et al., 1999). A subset of these genes, including *Prx1* and *Prx2*, *Alx3*, *Alx4*, and *Cart1*, are expressed during embryogenesis in similar patterns in neural crest-derived mesenchyme of developing craniofacial regions and in the mesenchyme of developing limbs (Leussink et al., 1995; Zhao et al., 1994; Qu et al., 1997; Ten Berge et al., 1998a). Mutant studies have established their partially redundant functions in these embryonic regions. For example,

studies of *Prx1/Prx2* double mutant mice demonstrated the roles of these genes in craniofacial and appendage development. These mutants have severe reductions of mandibular arch derived structures, and in the zeugopod of the limbs (Ten Berge et al., 1998b; Lu et al., 1999a; Lu et al., 1999b). On the basis of sequence similarity and embryonic expression patterns, *Alx3*, *Alx4* and *Cart1* appear to represent a distinct subgroup (Ten Berge, 1998a). Mice with mutations in *Alx4*, including the Strong's Luxoid (*lst*) alleles, have strong preaxial polydactyly, mild craniofacial abnormalities in anterior components of the skull base and parietal and frontal bones, as well as gastroschesis (Forsthoefel, 1963; Qu et al., 1997). *Cart1* mutant mice have major cranial defects including acrania and meroanencephaly (Zhao et al., 1996).

This study describes the generation and analysis of *Alx3* null mutant mice. *Alx3* single mutants appear to be normal, but *Alx3/Alx4* double mutant mice have severe craniofacial malformations that are never seen in *Alx4* single mutants.

Double mutants are born with midfacial clefting and many neural crest-derived skeletal elements are severely malformed. The anatomical abnormalities leading to the cleft nose phenotype are first detectable at E10.5 in medial craniofacial regions where *Alx3* and *Alx4* are strongly co-expressed. Although in wild-type embryos the medial nasal processes fuse at E11.5, in *Alx3*/*Alx4* double mutant embryos they develop in an abnormal lateral position, resulting in their failure to fuse. These defects correlate with abnormal and localised apoptosis at E10.0 in the nasal processes.

MATERIAL AND METHODS

Generation of the *Alx3* knock out construct

A fusion construct was made in pUC19 containing 3 kb *lacZ* coding sequence and a 3 kb loxP-pGK-TKNEOpA-loxP cassette that was transcribed in the reverse direction and flanked by loxP sites. A pUC19 vector containing pSDK-*lacZ* (gift of J. Rossant) was digested with *Kpn*I, blunted and ligated to *Not*I adaptors. Subsequently, the linearised fragment was digested with *Sma*I. The loxP-pGK-TKNEOpA-loxP cassette was isolated by digestion with *Not*I and *Sma*I of pHR56 (a gift from P. Kastner and F. Rijli) and was cloned into the linearised pUC19 vector containing pSDK-*lacZ*. In pBR-GEM11 (a gift from H. te Riele). The *Sal*I site in the polylinker was destroyed by partial *Sal*I digestion, filling in of the overhangs and re-ligation, generating pBR-GEM11Δ*Sal*I. Genomic fragments containing part of the *Alx3* gene (see Fig. 1) were isolated by screening of a 129 SVJ mouse genomic library cloned in phage lambda FIX® II vectors (Stratagene) with part of the *Alx3* cDNA. A 1.9 kb genomic *Alx3 Pst*I-*Nco*I fragment containing exon 2 was cloned in the pSDK-*lacZ*-loxP-pGK-TKNEOpA-loxP fusion construct, resulting in an in frame fusion of *Alx3* (exon 2) and *lacZ* sequences. The 7.4 kb *Not*I-*Sal*I fragment containing the *Alx3* (exon2)-*lacZ*-loxP-pGK-TKNEOpA-loxP cassette was ligated into the *Not*I and *Xho*I site of pBR-GEM11Δ*Sal*I. Finally, a 5.5 kb genomic *Sal*I fragment containing sequences 3′ of *Alx3* exon 4 was inserted into the *Xho*I site of *Alx3* (exon 2)-*lacZ*-loxP-pGK-TKNEO-pA-loxP-pBR-GEM11Δ*Sal*I, generating the complete targeting vector, p*Alx3*^{lacZ}, containing 1.9 kb 5′ and 5.5 kb 3′ homologous sequence to the *Alx3* locus (see Fig. 1).

Alx4 mutant

Strong's luxoid-J mice (official strain symbol Alx4$^{lst\text{-}J}$) were obtained from the Jackson Laboratory (Bar Harbor). These mice carry an *Alx4* allele containing a 16 bp deletion in the homeobox (Qu et al., 1998; Takahashi et al., 1998).

ES cell manipulation

A subclone from the E14 embryonic stem (ES) cell line was obtained from C. Brouwer, P. Krimpenfort and A. J. M. Berns (The Netherlands Cancer Institute, Amsterdam). 100 μg *Sal*I linearised p*Alx3*^{lacZ} was electroporated into 4×10^7 ES cells. The ES cells were grown on irradiated mouse embryonic fibroblasts (MEFs) in 10 ml GMEM containing 1000 units/ml leukaemia inhibiting factor (LIF) in a 5% CO_2 humidified incubator. From 2 days after electroporation, ES cells were selected in medium supplemented with 60% BRL-conditioned medium containing G418 (200 μg/ml) and LIF (1000 units/ml) without feeder cells to isolate 400 individual neomycin resistant clones. Targeted ES cell clones were identified for correct 3′ integration by digestion of their genomic DNA with *Stu*I. Southern analysis was performed using a unique *Nco*I-*Xho*I fragment of the 3′ *Alx3* locus. The *Nco*I-*Xho*I probe binds to sequences of a 9.5 kb fragment of the wild-type locus and to a 7.5 kb fragment of the mutant *Alx3* locus. Positive ES cell clones were subsequently checked for correct 5′ integration by digestion of their genomic DNA with *Eco*RI and Southern analysis using a unique *Sst*I-*Stu*I fragment of the 5′ *Alx*3 locus. The *Sst*I-*Stu*I probe binds to sequences of a 9.5 kb fragment of the wild-type locus and to an 11.5 kb fragment of the mutant *Alx3* locus (see Fig. 1).

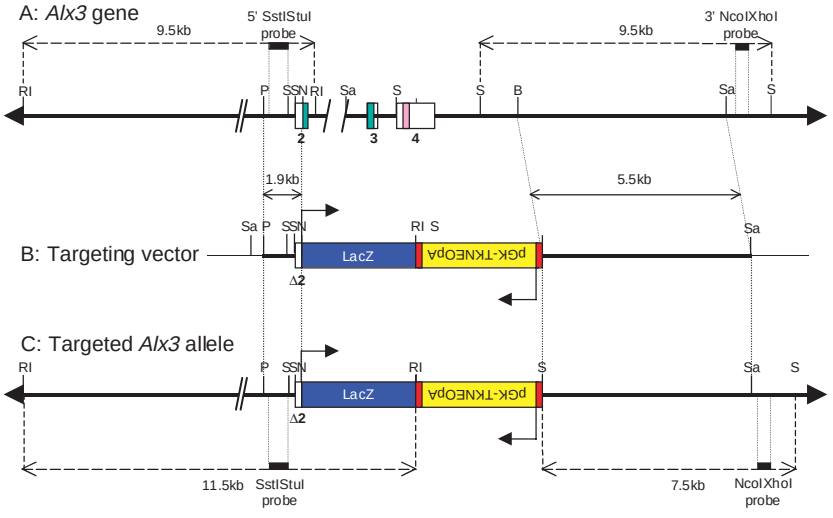

Fig. 1. Targeted mutagenesis of *Alx3*. (A) Structure of the *Alx3* locus: exon 2, 3 and 4 are depicted by open rectangles. The homeobox and the aristaless box (encoding the aristaless/OAR domain) are coloured. (B) Targeting vector: a 6 kb *lacZ*-loxP-pGK-TKNEOpA-loxP cassette was inserted in sequences of exon 2 upstream of the homeobox. 5′ 1.9 and 3′ 5.5 homologous sequences are indicated. Arrows in cassette indicate direction of transcription. (C) Targeted allele. The *Nco*I-*Xho*I probe corresponds to a region not present in the targeting construct, whereas the *Sst*I-*StuI* probe detects the short homology arm. Relevant restriction sites and probes are indicated. Restriction fragments for Southern analysis are indicated with broken arrows above wild-type *Alx3* allele and under targeted *Alx3* allele. Coloured boxes: black, probes; red, loxP sites; blue, *lacZ* cassette; yellow, pGK-TKNEOpA cassette; green, homeobox; pink, aristaless-box. Restriction sites: B, *Bam*HI; N, *Nco*I; P, *Pst*I; RI, *Eco*RI; S, *Stu*I; Sa, *Sal*I.

Generation and breeding of mutant mice

Chimaeric mice were obtained by injection of ES cells into C57BL/6 blastocysts. Chimaeric males were crossed with FVB/N females and heterozygous offspring was identified by coat colour and Southern analysis of tail DNA. Mice carrying the mutant *Alx3* allele were crossed to homozygosity. The *lst*^{J} mutant was obtained from the Jackson laboratory. This mutant has been shown to have a 16 bp deletion in the homeobox of the *Alx4* gene, resulting in loss of function (Qu et al., 1998). *Alx3*/*Alx4* double mutant mice were bred on a mixed genetic background with contributions of OLA/129, FVB/N, C57BL/6J and B6C3H.

All animal experiments were conducted under the approval of the animal care committee of the KNAW (Royal Dutch Academy of Arts and Sciences).

Genotyping

Genotyping was carried out using PCR on tail tip or yolk sac DNA. Amplification of 326 bp of the *Alx3* wild-type allele was performed by using: 5′-gaggctcaagaacaaggaagga-3′ (forward primer) and 5′-ctaggagcaggtcagagcaggaag-3′ (reverse primer). Amplification of 821 bp of the *lacZ* gene by using 5′-tcgagctgggtaataagcgttggcaat-3′ (forward primer) and 5′-agaccaactggtaatggtagcgac-3′ (reverse primer) was carried out to identify the mutant *Alx3* locus. Either 340 bp of the wild-type *Alx4* locus or 324 bp of the mutant *Alx4* locus was amplified using: 5′-caagccccctggaaaagacc-3′ (forward primer) and 5′-ggtacattgagttgtgctgtcc-3′ (reverse primer; Qu et al., 1998). To distinguish these products, they were restricted with *Pvu*II and the products were separated on a 3% agarose gel. The wild-type locus produces a 195 bp product and the mutant locus a product of 179 bp.

Analysis of embryos and newborn mice

Bone and cartilage staining was carried out according to a modified procedure of C. Fromental-Ramain (IGBMC, Strasbourg). Foetuses, and skinned and eviscerated new-born animals were fixed overnight in 96% ethanol, stained overnight for cartilage in 80% ethanol, 20% acetic acid + 0.5 mg/ml Alcian Blue (Sigma), rinsed twice in 96% ethanol for 3 hours and digested in 1.5% KOH for 2 hours, followed by bone staining in 0.5% KOH + 0.15 mg/ml Alizarin Red S (Sigma) overnight, destained in several changes of 20% glycerol + 1% KOH, and stored in 20% glycerol, 20% ethanol. Whole-mount X-Gal staining of E10.5 and E11.5 embryos was as described (Hogan et al., 1994). Whole-mount in situ hybridisation was performed as described (Leussink et al., 1995). Shh, Ptc and Fgf8 probes were kind gifts of C. Tabin (Boston, MA), R. Zeller (Utrecht) and G. R. Martin (San Francisco, CA), respectively. Sections hybridised with radioactive probes were photographed by double exposure of dark-field and bright-field images; a red filter was used during the dark-field exposure.

Cell proliferation was detected via analysis of BrdU incorporation into the DNA of dividing cells. Pregnant mice were treated with 1 ml 10 mM BrdU in PBS per 100 g body weight, and embryos were isolated 75 minutes later. Embryos were fixed overnight in 4% paraformaldehyde, dehydrated, embedded in paraffin and 4 μm thick sections were prepared according to standard techniques. Sections of each embryo were distributed over three parallel series of object glasses.

BrdU was detected using a fluorescein-labelled monoclonal anti-BrdU antibody (Roche) according to the instructions of the manufacturer. The signal was enhanced using the Alexa Fluor 488 signal amplification kit for fluorescein conjugated probes (Molecular Probes). Sections were counterstained with the fluorophore TO-PRO-3 (Molecular Probes), which stains nucleic acids. Each labelled section was scanned simultaneously for BrdU and TO-PRO-3 signals in two different channels using a Leica TCS NT confocal laser scanning microscope.

Apoptosis was detected by TUNEL assay using the In Situ Cell Death Detection KIT (AP) (Roche) according to the instructions of the manufacturer with some adaptations. The 4 μm sections were rehydrated and in contrast to the manufacturer's instructions sections were not treated with proteinase K. DNA was extended by terminal-deoxynucleotidyl transferase in the presence of fluorescein-labelled dUTP and incorporated fluorescein-labelled dUTP was subsequently detected with an anti-fluorescein antibody conjugated with alkaline phosphatase (AP). After substrate reaction with Fast Red apoptotic cells were detected using a light microscope.

RESULTS

Generation of *Alx3* mutants

Alx3 mutant mice were generated through homologous recombination in ES cells. The targeting strategy is shown in Fig. 1. A *lacZ* sequence linked to a pGK-TKNEO cassette was inserted in frame in a site 28 bp upstream of the homeobox. Upon recombination the mutant allele was expected to express a fusion protein consisting of the first 132 amino acids of the Alx3 protein and the β-galactosidase protein in a pattern identical to the *Alx3* expression pattern. LoxP sites flanked the selection cassette allowing its subsequent deletion from the allele. The mutant *Alx3* allele is expected to be functionally inactive as the protein encoded lacks both its conserved domains. Southern blotting using 3′ and 5′ probes confirmed successful targeting in at least 12 out of the 400 isolated ES cell clones (not shown). Three of these ES cell clones contributed to the germline of chimaeric mice generated by blastocyst injection. Heterozygous mice for the *Alx3* mutation appeared normal and were fertile. Two mouse lines were intercrossed and yielded wild-type, heterozygous and homozygous mutant offspring at the expected Mendelian frequencies. As the promoter region of the *Alx3* locus including the large first intron remains intact in the knock-in allele, no major differences are expected in the *lacZ* expression, when compared with *Alx3* mRNA expression. Analysis of the β-galactosidase expression pattern in heterozygous embryos of E9.5 to E12.5 showed essentially no differences with the endogenous *Alx3* expression pattern, confirming correct targeting of the gene (compare Fig. 2A with 2B for E10.5 embryos).

Alx3 null mice do not have obvious morphological abnormalities

Alx3 heterozygous and null mutant mice were born at expected frequencies and did not display noticeable abnormalities. They were fertile and appeared to have a normal lifespan. As *Alx3* is expressed predominantly in mesenchyme of developing limbs and craniofacial regions (Ten Berge et al., 1998a; Beverdam and Meijlink, 2001; Fig. 2) skeletons of null mutant newborn mice were thoroughly analysed, but no abnormalities were observed.

Abnormalities in *Alx3*/*Alx4* double mutant include severe craniofacial defects

Alx3 and *Alx4* encode highly related proteins (Qu et al., 1997; Ten Berge et al., 1998a); in addition, their expression patterns are highly similar, as we demonstrate in Fig. 2C-J (see also Beverdam and Meijlink, 2001). In facial primordia at early embryonic stages (Fig. 2C-H) there is considerable overlap of the expression domains, while the *Alx4* expression domain extends more laterally. In limb buds expression of both genes

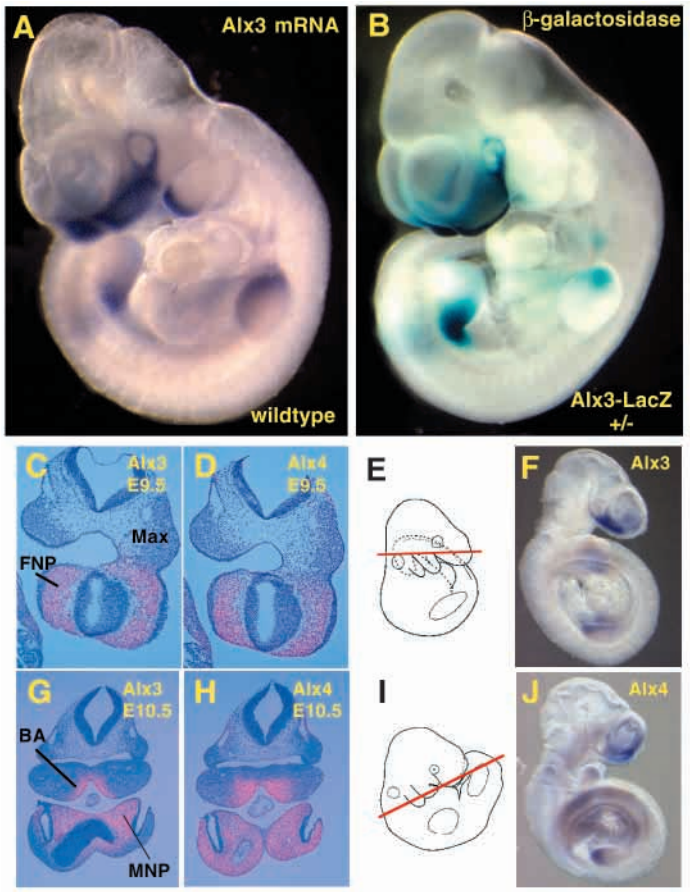

Fig. 2. Essentially correct *Alx3*/*lacZ* expression in knock-in mice; comparative expression analysis of *Alx3* and *Alx4* in E10.5 embryos. (A) Detection of *Alx3* mRNA (whole-mount in situ hybridisation) in whole embryo. (B) *lacZ* expression in $Alx3^{+/-}$ mouse embryo. Expression of *Alx3* and *lacZ* are qualitatively identical, confirming proper targeting of the *Alx3* locus. Staining in brain vesicles in A is background staining. (C,D) Radioactive in situ hybridisation showing overlapping expression of *Alx3* and *Alx4* in frontonasal processes (FNP) at E9.5. (G,H) Expression of Alx3 and Alx4 in medial nasal process (MNP) and mandibular arch (BA) at E10.5. (E,I) Schemes indicating approximate orientation of sections. (F,J) Whole-mount in situ hybridisation of E10.5 embryos showing overlap of expression in cranium and anterior mesenchyme of limbs.

is almost identical (Fig. 2F,J). It is therefore very likely that *Alx3* and *Alx4* have overlapping functions, and for that reason we decided to generate *Alx3/Alx4* double mutant embryos. We crossed *Alx3* mutants with Strong's luxoid Jackson ($Alx4^{lst\text{-}J}$) mice, that are known to carry a defective *Alx4* allele (Qu et al., 1998; Takahashi et al., 1998). *Alx4* mutants have preaxial polydactyly, abnormalities in the skull and frequently gastroschesis (Forsthoefel, 1963; Qu et al., 1997).

Alx4 single and $Alx3/Alx4^{lst\text{-}J}$ double mutant mice had preaxial polydactyly of the fore- and hindlimbs as described for *Alx4* mutant mice (see Fig. 3; Forsthoefel, 1963; Qu et al., 1997). Penetrance and severity of the *Alx4* phenotype are known to depend greatly on genetic background (Forsthoefel, 1968). In contrast to *Alx4/Cart1* double mutant mice (Qu et al., 1999), $Alx3/Alx4^{lst\text{-}J}$ double mutant had no significant aggravation of the polydactyly. We noted that both *Alx4* mutants and double mutants lacked the deltoid crests (arrows in Fig. 3A-C). These processes are located anteriorly on the humeri of normal forelimbs, and their absence may therefore be interpreted as a proximal expression of a mirror-image-duplication phenotype in the limb. This phenotype has not previously been described for any *Alx4* mutant, but has been found as an aspect of the extensive mirror image duplication that can be caused by *Hoxb8* overexpression (Charité et al., 1995). $Alx3/Alx4^{lst\text{-}J}$ double mutant mice had a reduction of the medial (sternal) end of the clavicle, a phenotype that is absent from the $Alx4^{lst\text{-}J}$ mutant (see arrowheads in Fig. 3A-F). Therefore in the shoulder girdle, but not in the limb itself, nor in the pelvic girdle, a function of *Alx3* was demonstrable.

Although in $Alx3^{+/-}/Alx4^{lst\text{-}J/+}$ mice no craniofacial abnormalities were detected and $Alx3^{+/+}/Alx4^{lst-J/\ lst\text{-}J}$ mutant mice had only relatively mild craniofacial abnormalities, $Alx3^{-/-}/Alx4^{lst-J/lst\text{-}J}$, $Alx3^{-/-}/Alx4^{lst\text{-}J/+}$ and $Alx3^{+/-}/Alx4^{lst-J/lst\text{-}J}$ mice had a broader and shorter cranium and displayed variable facial clefting comprising the entire nose region (see Fig. 4). Generally, they died within a few hours after birth with empty stomachs and air in their intestines, apparently as a consequence of craniofacial defects leading to inability to breath or owing to the ventral body wall defects as described for the *Alx4* mutant mouse (Qu et al., 1997). Eye lid abnormalities, as described by Forsthoefel (Forsthoefel , 1963) for *Strong's luxoid (Alx4)* mutants, seemed to be enhanced in double mutants. In $Alx3^{-/-}/Alx4^{lst-J/lst\text{-}J}$ newborn mice, the eyes were more often wide open (compare Fig. 4D with 4A-C). This aspect of the phenotype is apparently an indirect consequence of other cranial defects that make the eyes bulge out (Forsthoefel, 1963).

Most facial bones are malformed in *Alx3*/*Alx4* double mutant mice

We performed a detailed analysis of skulls of newborns with various double mutant genotypes using skeletal staining (Figs 5, 6) and histological sections (Fig. 7 for E12.5 and E13.5; see also Fig. 9 for earlier stages). A gradual increase in the severity of the phenotype was found, being weakest in the $Alx3^{+/+}/Alx4^{lst-J/lst\text{-}J}$ mutant mice and becoming progressively stronger in $Alx3^{-/-}/Alx4^{lst\text{-}J/+}$, $Alx3^{+/-}/Alx4^{lst-J/lst\text{-}J}$ and $Alx3^{-/-}/Alx4^{lst-J/lst\text{-}J}$ mutant mice, as demonstrated in Fig. 5. Double mutants displaying a mild phenotype had only a partially split nasal tip, but in mutants with extreme phenotypes, both lateral halves of the nose were anteriorly truncated and spaced wide apart. Most facial bones and many of the membranous bones of the vaults were affected in double mutants (compare in Fig. 6A,E with 6C,G). In homozygous *Alx4* mutant mice the parietal and frontal bones are reduced (See Fig. 5; Forsthoefel, 1963) and recent studies reveal that in humans, *ALX4* haploinsufficiency is associated with ossification defects in the parietal bones (Wuyts et al, 2000; Wu et al., 2000; Mavrogiannis et al., 2001). We observed in $Alx3/Alx4^{lst\text{-}J}$ double mutant newborn skulls an aggravation of the vault phenotype: besides a stronger reduction in the size of the frontal and parietal bones, the nasal bones were also affected, causing wide fontanels (compare Fig. 6A,B with 6C,D). The nasal capsule was divided in two separate halves both closed by remnants of the nasal septum while a medial nasal septum was absent (see white arrows in Fig. 5; Fig. 6C,G). The nasal labyrinths and the anterior part of the nasal capsule were

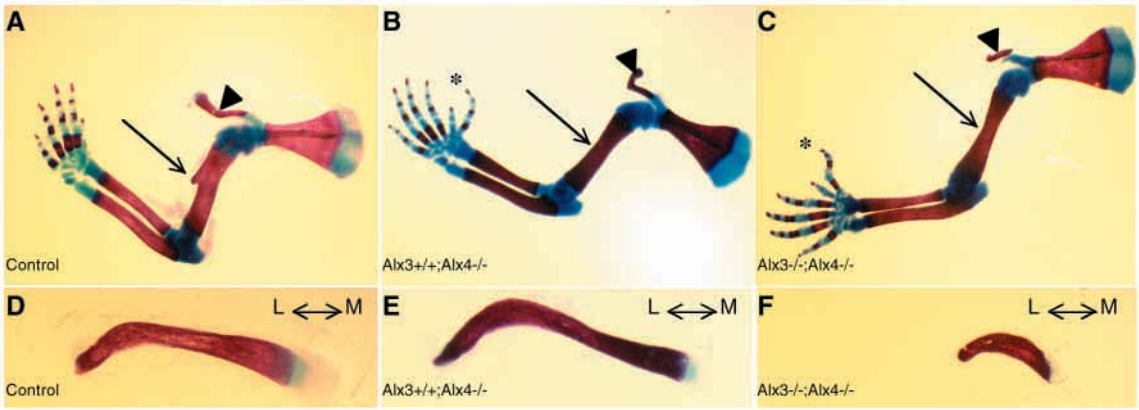

Fig. 3. Forelimb and pectoral girdle defects in *Alx* mutants. Alizarin Red (bone) and Alcian Blue (cartilage) stained forelimbs and pectoral girdles. Genotypes: (A,D) *Alx3*$^{+/-}$/*Alx4*$^{+/+}$; (B,E) *Alx3*$^{+/+}$/*Alx4*$^{lst\text{-}J/lst\text{-}J}$; (C,F) *Alx3*$^{-/-}$/*Alx4*$^{lst\text{-}J/lst\text{-}J}$. Arrowheads indicate the clavicle and arrows indicate (normal position of) deltoid crest. Asterisk marks extra digit in B,C. (D-F) Dissected clavicles; double arrows and L-M indicate lateral-medial orientation of the clavicles.

severely malformed and strongly curved (Fig. 5, lower panels; Fig. 7, compare A,E with B,F for the situation at E12.5 and E13.5). Also the premaxilla and maxilla were strongly affected and positioned abnormally laterally, and the palatine was cleft (Fig. 6, 'P' in F,H). In the mandible the distal part of the dentaries was truncated, but the incisors were normally present (see Fig. 5). The proximal part of the mandible seemed unaffected. The more lateral skull bones consisting of the alisphenoid bones and squamosal bones were malshaped and reduced (see structures marked 'As' and 'S' in Fig. 6F,H). The neural crest-derived skull base, consisting of the basipresphenoid and the pterygoid processes was also severely malformed and appeared broader (see green arrowheads in Fig. 5 and asterisks in Fig. 6E,G). More posterior skull structures derived from cephalic and somitic mesoderm like the posterior elements of the sphenoid bone, the occipital bone and the otic capsule, tympanic ring, inner and middle ear structures were normal in double mutants (see Figs 5-7). This region of the skull appears somewhat broader, which may be explained as a consequence of the anterior truncation of the skull that forces the more posterior skeletal elements outwards, in order to allow the brain to expand (Forsthoefel, 1963). Histological sections of E12.5 and E13.5 embryos demonstrate for these stages the normal morphology in posterior cranial structures, for example, the palatal processes and tongue in Fig. 7A-D), while more anteriorly the nasal cavities are malformed (arrows in Fig. 7A,B,E,F). Fig. 7G,H shows the cleft 'nasal septum'.

The skeletal elements derived from second and third arch mesenchyme, which form the hyoid skeleton were unaffected (not shown).

The abnormalities in *Alx3/Alx4* double mutants arise around E10.5

To define when the craniofacial defects in *Alx3*/*Alx4*$^{lst\text{-}J}$ double mutants first become apparent, control embryos and *Alx3*$^{-/-}$/*Alx4*$^{lst\text{-}J/+}$, *Alx3*$^{+/-}$/*Alx4*$^{lst\text{-}J/lst\text{-}J}$ and *Alx3*$^{-/-}$/*Alx4*$^{lst\text{-}J/lst\text{-}J}$ embryos were analysed from gestational day 9.5 to 15.5 (see Fig. 8).

At E9.5, craniofacial regions of wild-type embryos are composed of the primitive facial primordia that are arranged around the stomodaeum. The facial primordia consist of the frontonasal process and the protrusions of the first branchial arch. At E10.0 the nasal placodes become slightly indented, causing the formation of the medial and lateral nasal processes. Analysis of E9.5 and E10.0 *Alx3*$^{-/-}$/*Alx4*$^{-/-}$ whole-mount and sectioned embryos revealed no abnormalities in the first branchial arch or frontonasal processes (not shown). At E10.5 in normal embryos, the lateral and medial nasal processes enclose the nasal pits; the medial nasal processes will fuse in the midline around E11.5 forming the nasal septum. The primary palate is formed by fusion of the inferior borders of the medial nasal processes. From the medial walls of the maxillary processes palatal shelves grow out that fuse in the midline with the inferior border of the nasal septum, which grows down from the frontal

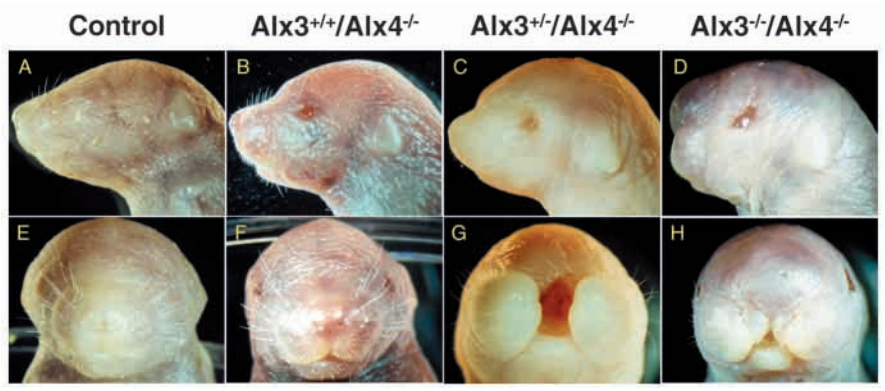

Fig. 4. Cranial phenotype of newborn *Alx3*/*Alx4*$^{lst\text{-}J}$ double mutant mouse. Lateral (A-D) and frontal (E-H) views on crania of *Alx3*$^{+/-}$ (A,E), *Alx4*$^{lst\text{-}J/lst\text{-}J}$ (B,F), *Alx3*$^{+/-}$/*Alx4*$^{lst\text{-}J/lst\text{-}J}$ (C,G) and *Alx3*$^{-/-}$/*Alx4*$^{lst\text{-}J/lst\text{-}J}$ (D,H) newborn mice. The anterior region is truncated, the nose is split and the eyes are open in all mutants. Note abnormal appearance of skull vault, owing to reduced parietal frontal and nasal bones in D. The severity of the cleft nose phenotype is highly variable.

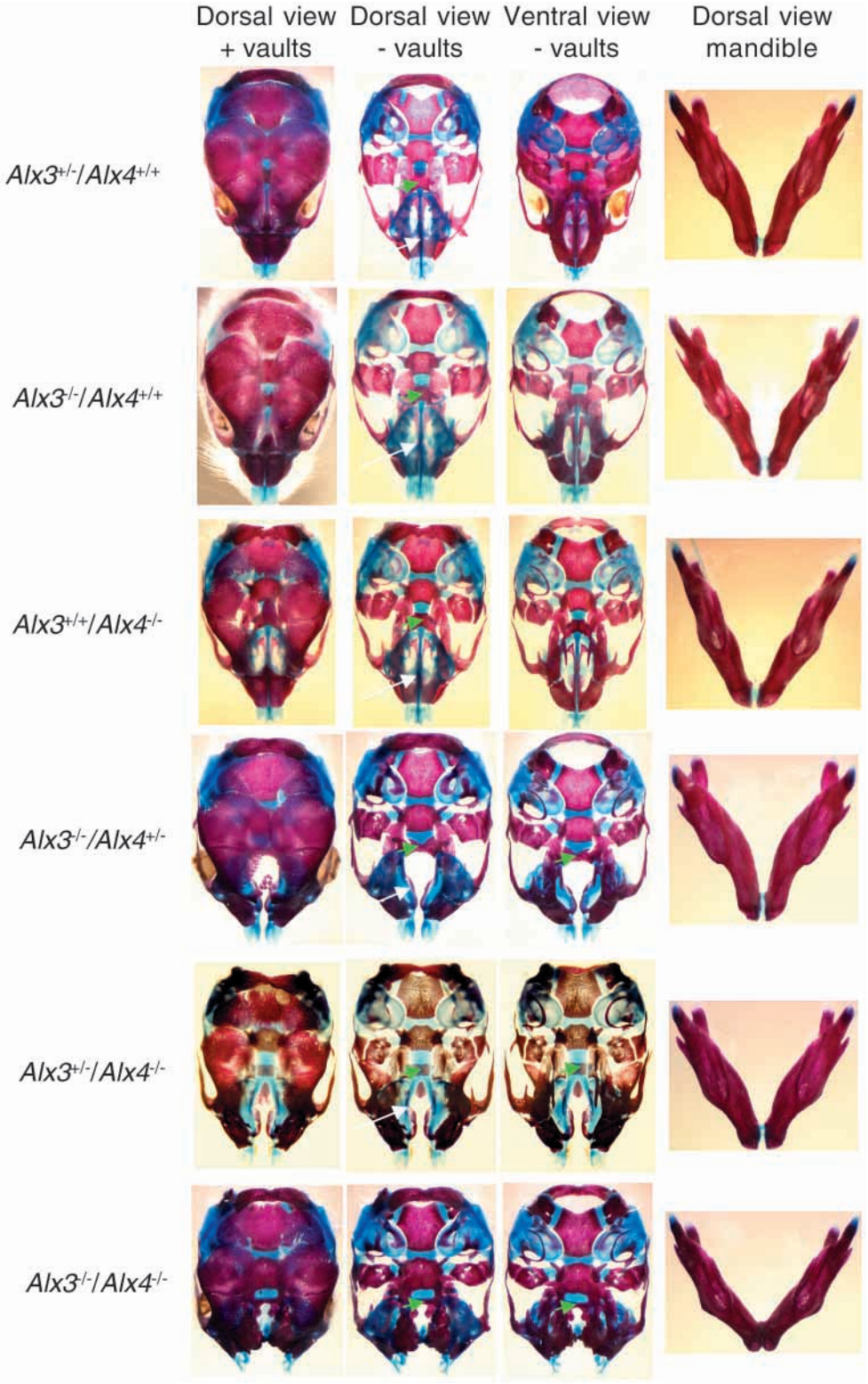

Fig. 5. Craniofacial abnormalities in *Alx3/Alx4*$^{lst\text{-}J}$ double mutant newborn mice. Alizarin Red (bone)/Alcian Blue (cartilage) stained skulls are shown. First column shows a dorsal view on the vaults of the skulls. Second column shows dorsal views on skulls from which vaults were dissected. Third column shows a ventral view on skulls from which mandibles and vaults were dissected. Fourth column shows the dissected mandibles. Genotypes are indicated to the left. Green arrows indicate the basipresphenoid, which constitutes the border of neural crest-derived skeletal elements and cephalic and somitic mesoderm derived skeletal elements. White arrows indicate the nasal septum.

process. Anteriorly, the shelves fuse with the primary palate resulting in the formation of the secondary palate.

In E10.5 *Alx3*$^{-/-}$/*Alx4*$^{lst\text{-}J/lst\text{-}J}$ embryos, the nasal processes are spaced more laterally than in wild-type embryos (compare arrowheads in Fig. 8A and 8E). The abnormally wide spacing became more pronounced later during development and resulted in defective merging of the nasal processes in the midline (compare arrowheads in Fig. 8B-D with 8F-H). Moreover, fusion of the maxillary processes with the lateral nasal processes occurred more laterally than in wild-type littermates, causing an abnormal shape and position of skeletal elements of the upper jaw. Fig. 7C,D,G,H (arrowheads) shows the presence of the nasal labyrinth, nasal septum remnants and vomeronasal organs within the unfused nasal processes in sections of E12.5 and E13.5 embryos. Instead of one medial mesenchymal condensation forming the cartilaginous nasal septum, two lateral condensations were detected, leaving an open space in the midline, which was continuous with the oral cavity owing to the cleft palate (Fig. 7E-H). In Fig. 8D,H, *lacZ* expression in E11.5 control embryos is shown to illustrate *Alx3* expression in the medial nasal processes; this domain becomes much wider in the double mutant. It thus appears that the defects observed in the *Alx3/Alx4*$^{lst\text{-}J}$ double mutant mice were directly or indirectly caused by the abnormal lateral position of the nasal processes in E10.5 embryos.

Gene expression in Alx mutants

As a next step to understand the basis of the Alx phenotype, we compared the expression in normal versus double mutant embryos of a number of selected genes in whole-mount or sectioned embryos of E9.5 to E11.5.

Shh is expressed in a distinct region of the ectoderm covering the medial nasal processes from E9.5 onwards (see arrow in Fig.

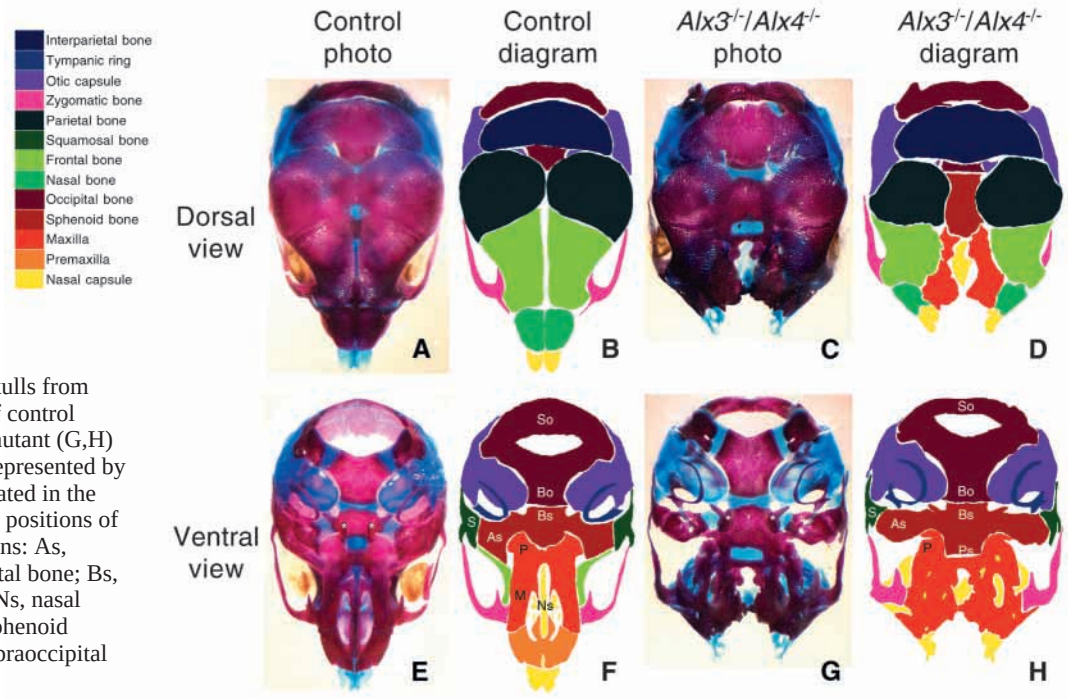

Fig. 6. Craniofacial abnormalities in *Alx3*$^{-/-}$/*Alx4*$^{lst\text{-}J/lst\text{-}J}$ double mutant newborn mice. Photos and corresponding diagrams of control and *Alx3/Alx4*$^{lst\text{-}J}$ double mutant skulls. Dorsal view on vaults of control (A,B) and *Alx3/Alx4*$^{lst\text{-}J}$ double mutant (C,D) skulls. Ventral views on skulls from which mandible was dissected of control (E,F) and *Alx3/Alx4*$^{lst\text{-}J}$ double mutant (G,H) mice. All skeletal elements are represented by a colour in the diagrams as indicated in the legend. Asterisks in E,G indicate positions of pterygoid processes. Abbreviations: As, alisphenoid bone; Bo, basioccipital bone; Bs, basisphenoid bone; M, maxilla; Ns, nasal septum; P, palatine; Ps, basipresphenoid bone; S, squamosal bone; So, supraoccipital bone.

9A). It is known to be upregulated in anterior limb bud mesenchyme of *Alx4* mutants (Chan et al., 1995), and downregulated in mandibular epithelium of *Prx1/Prx2* double mutants (Ten Berge et al., 2001). In double mutants at E10.5, but not at earlier stages, the expression domain in nasal epithelium is expanded to the same degree as the skull is wider (compare Fig. 9A with 9B,C). The expression pattern of the direct *Shh* target gene *Ptc* was changed accordingly (not shown). As the change of the expression pattern seems to follow the anatomical abnormalities, rather than vice versa, we do not believe that *Shh* and *Ptc* are downstream target genes of *Alx3* and *Alx4*, but rather that the changes in expression domains are secondary to the morphological changes. *Fgf8* is expressed in restricted regions in the oral ectoderm of the first branchial arch, in the ectoderm of the nasal pits and more distally in the medial nasal process ectoderm (see Fig. 9E). In *Alx3/Alx4*$^{lst\text{-}J}$ double mutant embryos of E9.5 to E11.5, we could not detect obvious changes in the *Fgf8* expression pattern (see Fig. 9E,F).

Pax9, *Prx3* and *Bmp2* have distinct expression patterns in mesenchyme of developing craniofacial primordia. We compared their expression domains in control embryos of E10.5 and E11.5 with those in *Alx3/Alx4*$^{lst\text{-}J}$ double mutant embryos. Fig. 9G-L shows the results for *Pax9*, known to have an important role in patterning of mesoderm and endoderm of the pharynx, and which is expressed in nasal, mandibular and maxillary processes. At E10.5 the expression patterns in control versus wild-type embryos are indistinguishable, while at E11.5 the changes observed appear to be a consequence of the anatomical abnormalities that are clearly visible around this stage. For example, *Pax9* is expressed laterally from the precartilage condensation in the midline of the nasal septum around the vomeronasal organs (Fig. 9H) and around the nasal cavities (Fig. 9I). In the highly abnormal nasal septum remnants the domain is split apart but essential characteristics, like its location with respect to the epithelium and surrounding the vomeronasal organs and nasal cavities appear to be retained (Fig. 9K,L). Similarly, *Bmp2* (not shown) and *Prx3* (Fig. 8M-R), a family member of the *Alx* genes also known as *Shot* or *OG-12*, which we selected because of the overlap of its expression domain with those of *Alx3* and *Alx4* in the medial nasal process, were normally expressed at E10.5, and at E11.5 in a way more or less predictable from the phenotype. This marker gene expression study therefore is informative because it contributes to the histological analysis of the mutant embryos, but does not provide clues as to the molecular mechanisms that underlie the phenotype.

Alx3 and *Alx4* control cell survival in the frontonasal mesenchyme at E10.0

To investigate the cellular basis of the facial phenotype of the *Alx3/Alx4*$^{lst\text{-}J}$ double mutant mice we performed BrdU incorporation assays to analyse proliferation patterns and TUNEL assays to detect apoptosis in embryos of around the developmental stages when the abnormalities first become obvious.

We studied cell proliferation in control and double mutant embryos of E9.5, E10.0 and E10.5. In both control and double mutant embryos, BrdU incorporation appeared highest in the mesenchymal cells flanking the deepening nasal placode and became lower towards more medial regions of the frontonasal process. We were not able to detect significant differences in proliferation rates between double mutant and control embryos (not shown).

We next studied apoptosis in transversal tissue sections of E9.5 and E10.0 control and double mutant embryos by performing TUNEL assays. In E9.5 embryos we did not observe any difference in cell death in control and double mutant embryos (not shown). In two double mutant embryos of E10.0, however, we observed two contralateral areas containing abnormally high numbers of apoptotic cells dorsolaterally in frontonasal mesenchyme adjacent to the placodes (Fig. 10A-G). We counted 30 adjacent 4 μm sections

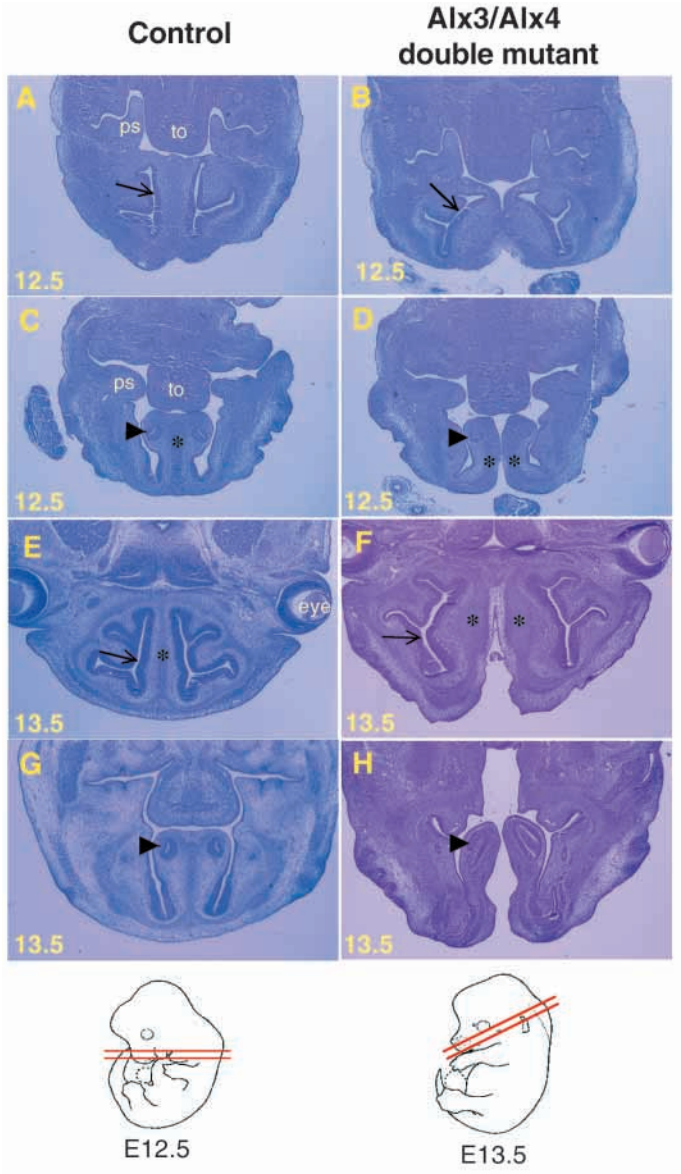

Fig. 7. Histological analysis of cranial phenotype. Transversal sections of wild-type (A,C,E,G) and *Alx3*$^{-/-}$/*Alx4*$^{lst\text{-}J/lst\text{-}J}$ (B,D,F,H) embryos. Stage (embryonic day) is indicated in lower left-hand corner. Asterisks, nasal septum precartilage condensation; arrows, nasal cavity; arrowheads, Jacobson's (vomeronasal) organ. Schemes below, with stages indicated, show approximate plane of section. Abbreviations: ps, palatal shelves; to, tongue.

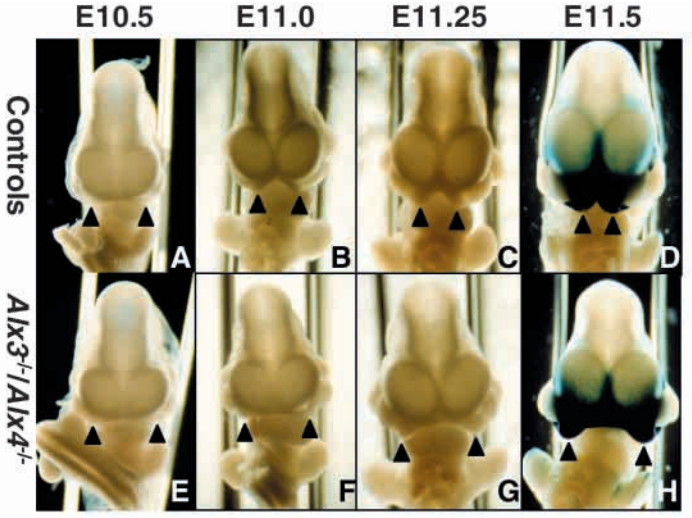

Fig. 8. Aetiology of the split nose phenotype. The nasal processes of *Alx3*/*Alx4*$^{lst\text{-}J}$ double mutant embryos fail to fuse around E11.5. Shown are frontal views on control (A-D; either *Alx3*$^{+/-}$ or wild type) and stage-matched *Alx3*/*Alx4*$^{lst\text{-}J}$ double mutant embryos (E-H) of E10.5 to E11.5 as indicated above photos. Posterior regions of most of the embryos were cut off to allow free view on the nasal processes. In embryos at E11.5, the *Alx3* expression domain was visualised by X-Gal staining to detect β-galactosidase. Arrowheads point to medial edges of the medial nasal processes, demonstrating the improper outgrowth and fusion of the nasal processes in double mutant embryos. Note the increasing difference in distance between the processes of control and *Alx3*/*Alx4*$^{lst\text{-}J}$ double mutant embryos.

in which the number of apoptotic cells was significantly higher compared with corresponding regions in five control embryos (compare Fig. 10B,E with 10A,D). The part of the frontonasal process where the apoptotic cells were observed falls within the region where *Alx3* and *Alx4* are both highly expressed (see Fig. 2C-H). This region contributes to the development of the nasal processes that will ultimately give rise to the nasal capsule, premaxilla and primary palate. In E10.5 embryos we detected essentially the same patterns of apoptotic cells in mutants and wild types. In the region presumably corresponding to the area where we saw the enhanced apoptosis in E10.0 embryos, we saw the same very low levels of TUNEL-positive cells in wild types and mutants (Fig. 10H,I). In E11.5 embryos, we did not see any TUNEL-positive cells in nasal mesenchyme (Fig. 10K,L).

We conclude that the lack of *Alx3* and *Alx4* early during craniofacial patterning leads to loss of cell survival in a confined area during a small time window. We deem it possible that this seemingly minor effect suffices to subsequently lead to abnormal outgrowth of the medial nasal processes. We propose that this early developmental anomaly contributes significantly to the rather dramatic phenotype seen in newborns.

DISCUSSION

We report that mice that lack the aristaless-related homeobox gene *Alx3* do not display anatomical abnormalities or diminished health. This suggested to us that loss of *Alx3* is compensated by genes with overlapping functions, which was confirmed when we analysed the phenotype of mice double mutant for *Alx3* and *Alx4*. These genes are structurally highly related and are expressed in similar expression patterns in developing embryos. *Alx4* loss-of-function mutants, including *Strong's luxoid* mutants and *Alx4*-targeted knockouts, have a complex phenotype including preaxial polydactyly, and mild abnormalities in the skull (Forsthoefel, 1963; Qu et al., 1998; Qu et al., 1999). Mice double mutant for *Alx3* and *Alx4*$^{lst\text{-}J}$ null alleles had severe abnormalities in the skull that are not seen in *Alx4* mutants, although other aspects of the *Alx4* phenotype were at the most marginally aggravated. *Alx3*/*Alx4*$^{lst\text{-}J}$ double mutants have severe clefting of the nose region. We noted the

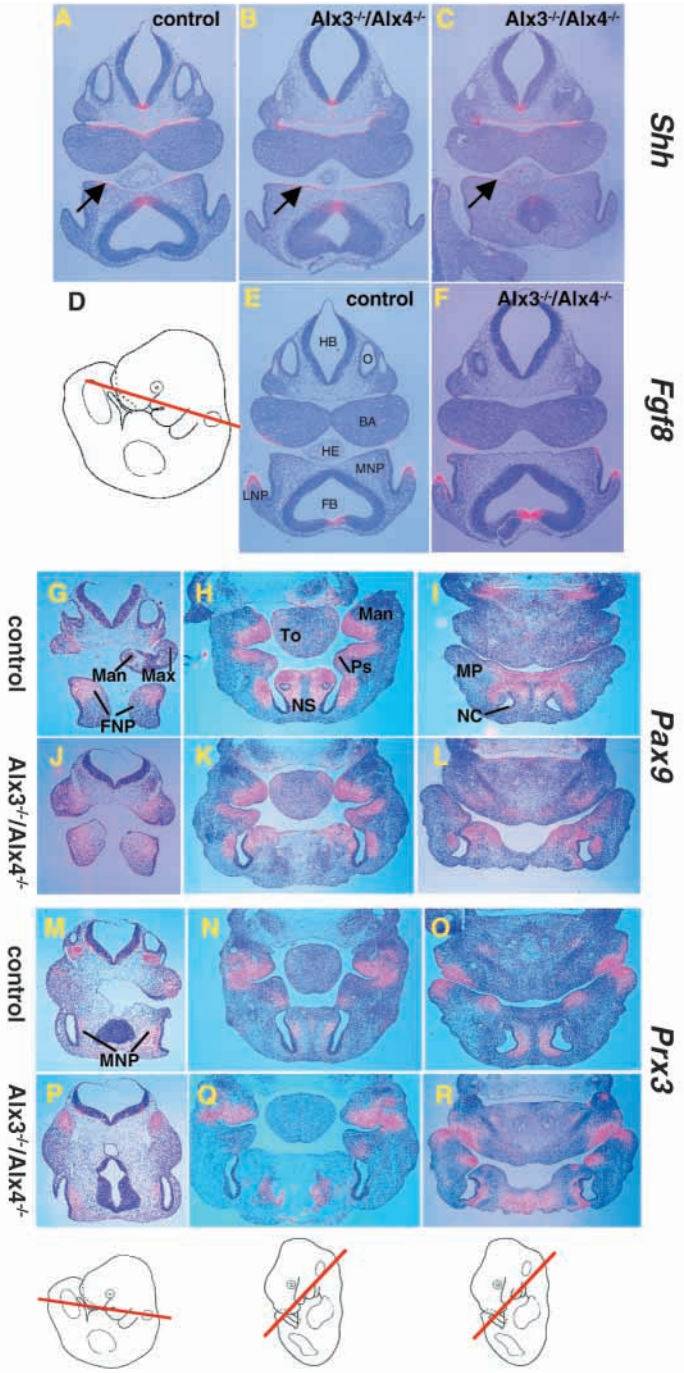

Fig. 9. Study of phenotype by analysis of expression patterns of marker genes in serial sections. Probes used are specified to the right. (A,E,G-I,M-O) Control embryos (either *Alx3* heterozygotes or wild type); (B,C,F,J-L,P-R) *Alx3*$^{-/-}$*Alx4*$^{lst\text{-}J/lst\text{-}J}$. (A-F) Serial sections of two E10.5 embryos and expression of ectodermal markers, where D is a scheme to indicate approximate plane of sections in the embryos used in this experiment. (G-R) Nearby serial sections of two control and two double mutant embryos and expression of two mesenchymal markers. (G,J,M,N) E10.5 embryos; (H,I,K,L,N,O,Q,R) Rather advanced E11.5 embryos. Orientation of sections of this series of embryos is depicted in lower row of panels. Arrows (in A-C) indicate *Shh* expression in ectoderm of the medial nasal processes. Abbreviations: BA, branchial (mandibular) arch; FB, forebrain; FNP frontonasal process; HB, hindbrain; HE, heart; Man, max, mandibular and maxillary process, respectively, of first branchial arch; MNP, medial nasal process; MP, maxillary process; NC, nasal cavity; NS, nasal septum; O, otocyst; Ps, palatal shelf (part of maxilla); To, tongue.

earliest signs of anatomical abnormalities in the head region around gestational day 10.5, when the nasal processes grew out abnormally laterally. The wide lateral spacing of the processes resulted in failure to fuse, and ultimately in the cleft nose phenotype in newborn mice. Analyses of cellular parameters in early double mutant embryos demonstrated increased cell death in restricted regions of the presumptive nasal processes, which is most likely causally linked to the subsequent abnormal morphogenesis of the nasal processes.

Overlapping functions of *Alx3*, *Alx4* and *Cart1*

Alx3 and *Alx4* are expressed in overlapping domains in neural crest-derived mesenchyme of medial regions of the developing facial primordia (Qu et al., 1997; Ten Berge et al., 1998). These regions grow out to form the cartilages, bones and connective tissues of the face and the most anterior part of the skull base.

Cart1 is a third protein that is highly related to Alx3 and Alx4. These three proteins share very similar homeodomains, a common C-terminal domain called aristaless- or OAR domain, and additional sequence similarity between these two domains that sets them apart at the structural level from other aristaless-related proteins. *Cart1* expression in craniofacial regions is spatially and temporally similar to that of *Alx3* and *Alx4*, but *Cart1* expression is detectable earlier in the head mesenchyme. *Cart1* mutant mice have a strong cranial phenotype caused by cranial neural tube closure defects that lead to acrania and meroanencephaly at the time of birth (Zhao et al., 1996). In addition, these mice have other, relatively mild craniofacial defects. It is striking that, like *Alx3/Alx4*$^{lst\text{-}J}$ mutants, *Alx4*/*Cart1* double mutant mice have severe midfacial clefting and distally truncated mandibles (Qu et al., 1999). In contrast to our conclusions on the early anatomical basis of the cleft-nose phenotype of the *Alx3/Alx4*$^{lst\text{-}J}$ mutants, the phenotype of the *Alx4/Cart1* double mutant mice has been explained as a failure of the ‘nasal cartilages to fuse’ (Qu et al., 1999). In view of the similar molecular basis of the defect in both cases, we consider it quite likely, however, that in both double mutants the anatomical basis of the phenotype is the same. We have shown that the critical stage in the aetiology of the phenotype occurs before cartilage differentiation and even mesenchyme condensation. Unfortunately, no embryonic stages of *Alx4/Cart1* double mutants have been described (Qu et al., 1999).

Comparison of the *Alx4*$^{lst\text{-}J}$ single mutants and *Alx3/4*$^{lst\text{-}J}$ double mutants showed a strong exacerbation of the phenotype in craniofacial, but not in other regions. The striking *Alx4* expression pattern anteriorly in limb bud mesenchyme is also found for *Alx3*, so it is unexpected that in *Alx3/Alx4*$^{lst\text{-}J}$ double mutants no enhancement of the phenotype is seen. Apparently, in *Alx4* mutants, Alx3 can not compensate to a significant extent the function of Alx4. Strikingly, mutation of *Cart1* has been shown to clearly exacerbate the polydactyly of *Alx4* mutants (Qu et al., 1999). We have recently shown that *Cart1* is expressed at low level in anterior limb bud mesenchyme at E9.5-E10.5 (Beverdam, and Meijlink, 2001). It seems

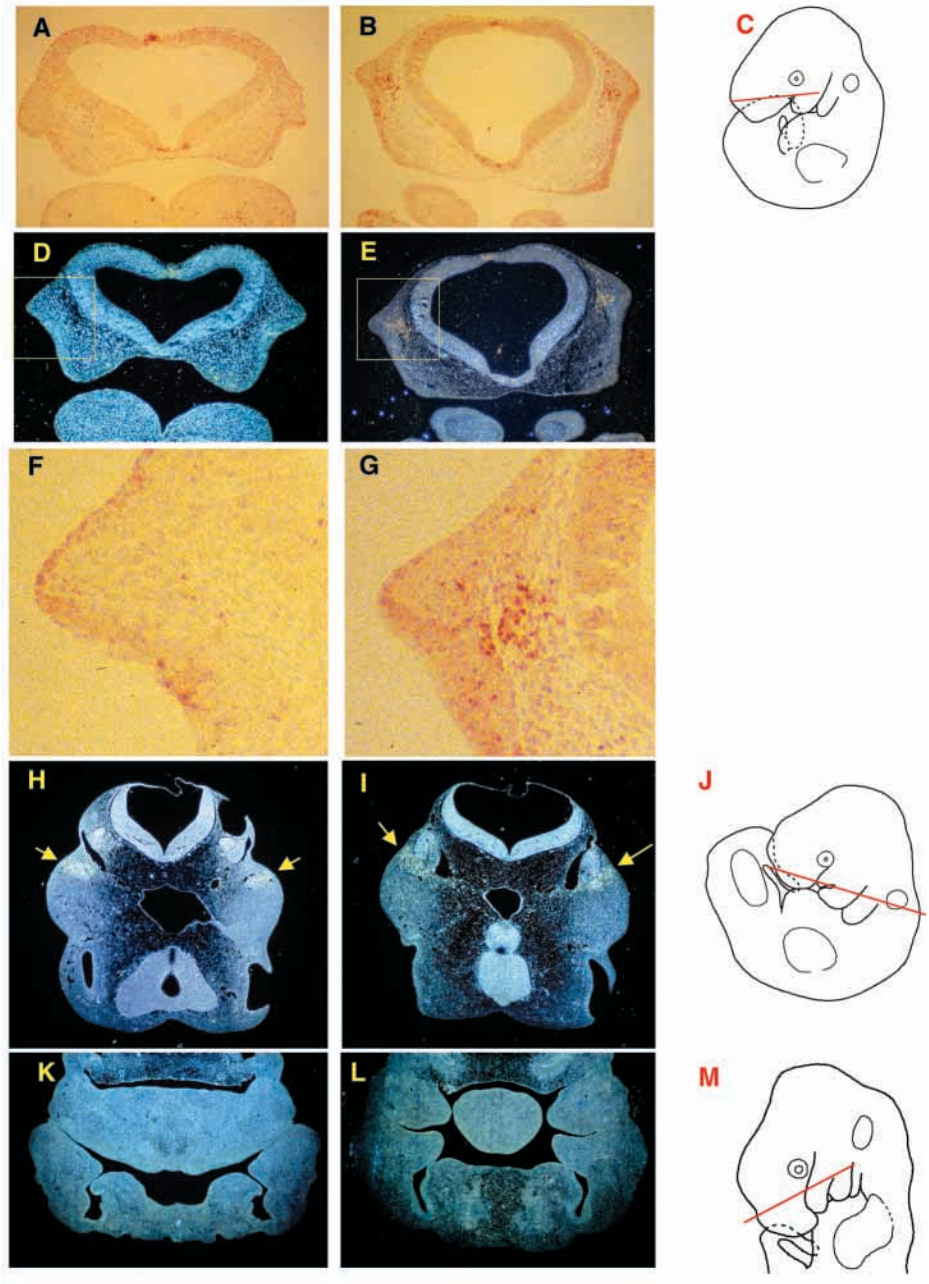

Fig. 10. Apoptosis in *Alx3*/*Alx4*$^{lst\text{-}J}$ double mutant embryos. In a restricted region of the frontonasal process of *Alx3*/*Alx4*$^{lst\text{-}J}$ double mutant embryos, a significant number of mesenchymal cells undergo apoptosis compared with stage-matched control embryos. (A,D,F,H,K) control embryos (wild-type or *Alx3*$^{+/-}$); (B,E,G,I,L) embryos of double mutant embryos; (C,J,M) schemes depicting plane of sections of embryos shown to their left. TUNEL assays were carried out to detect apoptosis. Positive cells appear red in this assay, as seen in brightfield images (A,B,F,G). Because of difficulty with visualising TUNEL staining simultaneously with histology, we show also darkfield images where positive cells appear as white to orange spots. The yellow squares in D,E mark the crucial area where we found differences in apoptosis in E10.0 embryos. These areas are shown enlarged, and in brightfield, in F,G. No or very few apoptotic cells were detected in the vicinity of the nasal processes of embryos of E10.5 and E11.5. The yellow arrows in panels H,I indicate apoptopic areas in the maxillary component of the first branchial arch, confirming that the negative result in this experiment was not due to technical failure.

contradictory that low expression of *Cart1* has more impact than that of Alx3; this paradox may be solved by taking into account possible specific functional properties of heterodimers probably formed by Alx3, Cart1 and Alx4 with each other and with other paired-related homeodomains (Qu et al., 1999; Tucker and Wisdom, 1999). It remains possible that in yet to be made *Alx3/Alx4/Cart1* triple mutants, preaxial polydactyly is further aggravated. The expression patterns of *Alx3*, *Alx4* and *Cart1* do not straightforwardly suggest an explanation for Alx3 being apparently more important in the cranium than in the limbs. This explanation should perhaps be sought for in differences in interactions with other genes in these areas.

The only defect outside the skull exclusively found in the double mutant was the truncation of the clavicle. We previously noted *Alx3* expression in the developing clavicle (shown in Ten Berge et al., 1998a; A. B., unpublished). The embryological origin of the clavicle is obscure, but recent evidence suggests that there is some neural crest contribution to the clavicle, in particular the site of the attachment point for the cleidohyoid muscle (McGonnell et al., 2001). This suggests that the lost piece of the clavicle is at least partly neural crest derived. It is striking that the function of *Alx3* is almost exclusively manifest in the craniofacial areas where it appears to control morphogenesis of neural crest-derived skeletal elements, and that this exception concerns a structure also linked to neural crest-derived mesenchyme. It should be noted that the clavicle, the only remaining dermal bone of the mouse pectoral girdle, evolved originally as part of the head (discussed in McGonnell et al., 2001; Torrey, 1978)

As *Alx3* is highly expressed in the body wall, gastroschesis was expected to increase in double mutants, but no significant differences in penetrance or severity were observed. It should

be noted that a quantitatively accurate comparison of phenotypes is hampered by the heterogeneous genetic background of the mice used for the analysis and the sensitivity of *Alx4* mutations for genetic background effects (Forsthoefel, 1968).

The data discussed here indicate that *Alx3*, *Alx4* and *Cart1* constitute a distinct subgroup of genes sharing identical or very similar roles in the patterning of the facial primordia, in particular the nasal process. A second subgroup of aristaless-like genes consists of *Prx1* and *Prx2*, which share to some extent the characteristics of structure and expression of the *Alx3/4* and *Cart1* genes, but have functions that are primarily vital to correct patterning of the mandibular arch and consequently the formation of the jaws.

Alx3 and *Alx4* are required for proper outgrowth of the nasal processes

We determined that the abnormalities in *Alx3/Alx4*$^{lst\text{-}J}$ double mutant embryos first become obvious around E10.5 in development, when the nasal processes become prominent structures. In double mutant embryos of E10.5, the nasal processes develop too wide apart and therefore fail to fuse at around E11.5, eventually causing a wide midline cleft by the time of birth. The crucial process of fusion of the facial primordial processes depends heavily on their proper outgrowth and morphogenesis. A lack of critical mass, or their abnormal position is likely to jeopardise the fusion process (discussed by Thorogood, 1997).

Within the nasal processes, most structures, including the nasal cavities, continue to develop in a relatively normal way, suggesting that most morphogenetic processes that regulate proliferation and differentiation of cells in the nose region do not depend on *Alx3* or *Alx4*. To obtain clues at a molecular level on the nature of the defects, and in the hope of identifying target genes, we studied the expression pattern of several genes known to have distinct expression patterns in the facial regions, generally with negative results. *Shh*, which has been implicated in the outgrowth of facial processes (Hu and Helms, 1999), is expressed in normal embryos in a restricted pattern in the facial ectoderm covering the frontonasal and the medial nasal processes, and Ptc, a direct downstream *Shh* target, is expressed in ectoderm as well as mesenchyme that underlies the *Shh*-expressing ectoderm. We found that in double mutant embryos of E10.5, but not at earlier stages, the region of ectodermal cells expressing *Shh* had expanded and *Ptc* expression in ectoderm and mesenchyme had changed accordingly. As the aberrant expression seems to occur only after the emergence of anatomical abnormalities, it appears that this expansion is a result rather than a cause of the malformations, and there is no reason to suggest that *Shh* is a specific target of *Alx* genes. Conceivably, the ectopic *Shh* expression from E10.5 onwards contributes to the aetiology of the phenotype.

Alx3, *Alx4* and *Cart1* and apoptosis

To understand at a cellular level the basis of the aberrant anatomy of E10.5 double mutants, we analysed cellular processes underlying growth of the nasal prominences by measuring proliferation and cell death patterns in embryos of these and earlier stages. We could not detect significant differences in proliferation, indicating that the defects are not caused by proliferation defects. We cannot, however, exclude the possibility that changes in proliferation too subtle to be detected in our assays do account for significant morphological defects.

In double mutant embryos at E10.0, but not at earlier or later stages, we did detect apoptosis in a very restricted region in the mesenchyme of the outgrowing frontonasal process where in control embryos of the same developmental stage no or very little apoptosis was detected. Apoptosis in double mutants was restricted to a region located dorsally within the process where *Alx3* and *Alx4* are both expressed. Lineage studies performed by McGonnell et al. (McGonnell et al., 1998) suggest that this region will contribute to the medial nasal processes. It is conceivable that local cell death in an outgrowing process leads to its subsequent malpositioning and therefore that the aberrant apoptosis seen in the *Alx3/4* mutant is likely to be in part responsible for the later defects. It remains currently unclear which pathway links the expression of these transcription factors to the process of apoptosis. A causal link between aristaless-related genes and regulated cell death is not without precedent. In *Cart1* mutants, 70% of E8.75 embryos have an anterior neural tube closure defect that appears to result from increased cell death in the mesenchyme surrounding the forebrain vesicles (Zhao et al., 1996). These results suggest that the *Alx/Cart* subgroup regulates craniofacial patterning by mechanisms that involve control of cell survival.

Hierarchy of genes controlling craniofacial development

Our understanding of the molecular basis of craniofacial patterning is rapidly expanding. From gastrulation onwards Hox genes pattern the embryo along the anteroposterior axis from posterior up to the hindbrain regions. Formation and regionalisation of more rostral head structures, on the other hand, is dependent on genes like *Otx1* and *Otx2* and *Emx1* and *Emx2*, which are expressed in nested patterns in mid- and forebrain before and during cephalic neural crest cell migration (Kuratani et al., 1997; Cecchi and Boncinelli, 2000). These genes may to some extent be responsible for determining genetic identity and preprogramming of these neural crest cells, which ultimately will populate the branchial arches and the frontonasal process. In a genetic hierarchy that appears to regulate craniofacial patterning, downstream from these neural genes, other gene families, including those related to *Distal-less* and *aristaless*, have local functions in patterning neural crest-derived mesenchyme. It appears that the two subgroups of aristaless-like genes that we distinguish exercise their function on different but slightly overlapping complementary anteroposterior levels. The most important defects in *Prx* mutants are in the derivatives of the distal mandibular arch that is populated by neural crest derived from the anterior hindbrain (Ten Berge et al., 1998; Lu et al., 1999a). By contrast, *Alx3*, *Alx4* and *Cart1* control patterning of the medial regions of the anterior skull base and of the nose and upper jaw regions (Qu et al., 1999; this paper); these structures derive from midbrain neural crest. In agreement with this, *Otx2* heterozygous mutants have defects in similar regions of the anterior skull base and distal jaws (Kuratani et al., 1997). In future research, we will test our hypothesis that *Alx* and *Prx* genes are directly or indirectly regulated by *Otx2* and a rhombomere 1- and

rhombomere 2-specific gene like *Gbx2*, respectively (Wassarman et al., 1997).

We thank Jacqueline Deschamps, Christine Mummery, Ronald Plasterk, Rolf Zeller and the anonymous referees for constructive criticism. We acknowledge Fons Verbeek and Marjo den Broeder for kindly helping preparing the diagrams of Fig. 6 and Willem Hage for help with analysis of proliferation assays. We thank Anthony Graham for communicating information before publication. We also thank Carla Kroon for technical assistance, Ferdinand Vervoordeldonk and Jaap Heinen for help in preparing the illustrations, and the animal care unit for their contributions.

REFERENCES

Beverdam, A. and Meijlink, F. (2001). Expression patterns of group-I aristaless-related genes during craniofacial and limb development. *Mech. Dev.* **107**, 163-167.

Cecchi, C. and Boncinelli, E. (2000). Emx homeogenes and mouse brain development. *Trends Neurosci.* **23**, 347-352.

Chan, D. C., Laufer, E., Tabin, C. and Leder, P (1995). Polydactylous limbs in Strong's Luxoid mice result from ectopic polarizing activity. *Development* **121**, 1971-1978.

Charité, J., De Graaff, W., Shen, S. B. and Deschamps, J. (1994). Ectopic expression of Hoxb-8 causes duplication of the ZPA in the forelimb and homeotic transformation of axial structures. *Cell* **78**, 589-601.

Couly, G. F., Coltey, P. M. and Le Douarin, N. M. (1993). The triple origin of skull in higher vertebrates: a study in quail-chick chimeras. *Development* **117**, 409-429.

Ferguson, C. A., Tucker A. S. and Sharpe, P. T. (2000). Temporospatial cell interactions regulating mandibular and maxillary arch patterning. *Development* **127**, 403-412.

Forsthoefel P. F. (1963). The embryological development of the effects of Strong's Luxoid gene in the mouse. *J. Morphol.* **113**, 427-452.

Forsthoefel P. F. (1968). Responses to selection for plus and minus modifiers of some effects of Strong's luxoid gene on the mouse skeleton. *Teratology* **1**, 339-351.

Hogan, B., Beddington, R., Costantini, F. and Lacy, E. (1994). *Manipulating the mouse embryo*. 2nd edn. New York: Cold Spring Harbor Laboratory Press.

Hu, D and Helms, J. A. (1999). The role of sonic hedgehog in normal and abnormal craniofacial morphogenesis *Development* **126**, 4873-4884.

Kuratani, S., Matsuo, I. and Aizawa, S. (1997). Developmental patterning and evolution of the mammalian viscerocranium: genetic insights into comparative morphology. *Dev. Dyn*. **209**, 139-155.

Le Douarin, N. M., Ziller, C. and Couly, G. F. (1993). Patterning of neural crest derivatives in the avian embryo: in vivo and in vitro studies. *Dev. Biol*. **159**, 24-49.

Leussink, B., Brouwer, A., el Khattabi, M., Poelmann, R. E., Gittenberger-de Groot, A. C. and Meijlink, F. (1995). Expression patterns of the paired-related homeobox genes MHox/Prx1 and S8/Prx2 suggest roles in development of the heart and the forebrain. *Mech. Dev.* **52**, 51-64.

Lu, M. F., Cheng, H. T., Kern, M. J., Potter, S. S., Tran, B., Diekwisch, T. G. and Martin, J. F. (1999a). Prx-1 functions cooperatively with another paired-related homeobox gene, prx-2, to maintain cell fates within the craniofacial mesenchyme. *Development* **126**, 495-504.

Lu, M. F., Cheng, H. T., Lacy, A. R., Kern, M. J., Argao, E. A., Potter, S. S., Olson,E. N. and Martin, J. F. (1999b). Paired-related homeobox genes cooperate in handplate and hindlimb zeugopod morphogenesis. *Dev. Biol*. **205**, 145-157.

Mavrogiannis, L. A., Antonopoulou, I., Baxova, A., Kutilek, S., Kim, C. A., Sugayama, S. M., Salamanca, A., Wall, S. A., Morriss-Kay, G. M. and Wilkie, A. O. (2001). Haploinsufficiency of the human homeobox gene ALX4 causes skull ossification defects. *Nat. Genet.* **27**, 17-18.

McGonnell, I. M., Clarke, J. D. and Tickle, C. (1998). Fate map of the developing chick face: analysis of expansion of facial primordia and establishment of the primary palate. *Dev. Dyn.* **212**, 102-118.

McGonnell, I. M., McKay, I. J. and Graham, A. (2001). A population of caudally migrating cranial neural crest cells; functional and evolutionary implications. *Dev. Biol.* **236**, 354-363.

Meijlink, F., Beverdam, A., Brouwer, A., Oosterveen, T. C. and Ten Berge, D. (1999). Vertebrate *aristaless*-related genes. *Int. J. Dev. Biol.* **43**, 651-663.

Qu, S., Niswender, K. D., Ji, Q. S., van der Meer, R., Keeney, D., Magnuson, M. A. and Wisdom, R. (1997). Polydactyly and ectopic ZPA formation in Alx-4 mutant mice. *Development* **124**, 3999-4008.

Qu, S., Tucker, S. C., Ehrlich, J. S., Levoirse, J. M., Flaherty, L. A., Wisdom, R. and Vogt, T. F. (1998). Mutations in mouse aristaless-like4 cause Strong's Luxoid polydactyly. *Development* **125**, 2711-2721.

Qu, S., Tucker, S., Zhao, Q., DeCrombrugghe, B. and Wisdom, R. (1999). Physical and genetic interactions between *Alx4* and *Cart1*. *Development* **126**, 359-369.

Richman, J. M. and Tickle, C. (1992). Epithelial-mesenchymal interactions in the outgrowth of limb buds and facial primordia in chick embryos. *Dev. Biol.* **54**, 299-308.

Schilling, T. F. (1997). Genetic analysis of craniofacial development in the vertebrate embryo. *BioEssays* **19**, 459-468.

Takahashi, M., Tamura, K., Buscher, D., Masuya, H., Yonei-Tamura, S., Matsumoto, K., Naitoh-Matsuo, M., Takeuchi, J., Ogura, K., Shiroishi, T., Ogura, T. and Izpisúa-Belmonte, J. C. (1998). The role of Alx-4 in the establishment of anteroposterior polarity during vertebrate limb development. *Development* **125**, 4417-4425.

Ten Berge, D., Brouwer, A., el Bahi, S., Guénet, J. L., Robert, B. and Meijlink, F. (1998a). Mouse Alx3: An aristaless-like homeobox gene expressed during embryogenesis in ectomesenchyme and lateral plate mesoderm. *Dev. Biol.* **199**, 11-25.

Ten Berge, D., Brouwer, A., Korving, J., Martin, J. F. and Meijlink, F. (1998b). Prx1 and Prx2 in skeletogenesis: roles in the craniofacial region, inner ear and limbs. *Development* **125**, 3831-3842.

Ten Berge, D., Brouwer, A., Korving, J., Reijnen, M. J., Van Raaij, E. J., Verbeek, F., Gaffield, W. and Meijlink, F. (2001). *Prx1* and *Prx2* are upstream regulators of *sonic hedgehog*, and control cell proliferation during mandibular arch morphogenesis. *Development* **128**, 2929-2938.

Thorogood, P. (1997). The head and face. In *Embryos, Genes and Birth Defects* (ed. P. Thorogood), pp. 197-229. Chichester: John Wiley & Sons.

Torrey, T. W. (1978). *Morphogenesis of the Vertebrates*. New York: Wiley.

Tucker, S. C. and Wisdom, R. (1999). Site-specific heterodimerization by paired class homeodomain proteins mediates selective transcriptional responses. *J. Biol. Chem.* **274**, 32325-32332.

Wassarman, K. M., Lewandoski, M., Campbell, K., Joyner, A. L., Rubenstein, J. L., Martinez, S. and Martin, G. R. (1997). Specification of the anterior hindbrain and establishment of a normal mid/hindbrain organizer is dependent on Gbx2 gene function. *Development* **124**, 2923-2934.

Wedden, S. E. (1987). Epithelial-mesenchymal interactions in the development of chick facial primordia and the target of retinoid action. *Development* **99**, 341-351.

Wu, Y. Q., Badano, J. L., McCaskill C., Vogel H., Potocki L. and Shaffer L. G. (2000). Haploinsufficiency of ALX4 as a potential cause of parietal foramina in the 11p11.2 contiguous gene-deletion syndrome. *Am. J. Hum. Genet.* **67**, 1327-1332.

Wuyts, W., Cleiren, E., Homfray, T., Rasore-Quartino, A., Vanhoenacker, F. and Van Hul, W. (2000). The ALX4 homeobox gene is mutated in patients with ossification defects of the skull. *J. Med. Genet.* **37**, 916-920.

Zhao, G. Q., Eberspaecher, H., Seldin, M. F. and DeCrombrugghe, B. (1994). The gene for the homeodomain-containing protein Cart-1 is expressed in cells that have a chondrogenic potential during embryonic development. *Mech. Dev*. **48**, 245-254.

Zhao, Q., Behringer, R. R. and DeCrombrugghe, B. (1996). Prenatal folic acid treatment suppresses acrania and meroanencephaly in mice mutant for the *Cart1* homeobox gene. *Nat. Genet*. **13**, 275-283.